

Phenomenological description of the microwave surface impedance and complex conductivity of high- T_c single crystals

M. R. Trunin and Yu. A. Nefyodov

Institute of Solid State Physics, 142432 Chernogolovka, Moscow district, Russia

Herman J. Fink

Department of Electrical and Computer Engineering, University of California, Davis, California 95616, USA

(July 6, 2018)

Measurements of the microwave surface impedance $Z_s(T) = R_s(T) + iX_s(T)$ and of the complex conductivity $\sigma_s(T)$ of high-quality, high- T_c single crystals of YBCO, BSCCO, TBCCO, and TBCO are analyzed. Experimental data of $Z_s(T)$ and $\sigma_s(T)$ are compared with calculations based on a modified two-fluid model which includes temperature-dependent quasiparticle scattering and a unique temperature variation of the density of superconducting carriers. We elucidate agreement as well as disagreement of our analysis with the salient features of the experimental data. Existing microscopic models are reviewed which are based on unconventional symmetry of the order parameter and on novel mechanisms of quasiparticle relaxation.

I. INTRODUCTION

High-precision microwave measurements of the temperature dependence of the surface impedance $Z_s(T) = R_s(T) + iX_s(T)$ of high- T_c superconductors (HTS's) advance considerably our understanding of pairing of superconducting electrons in these materials. In particular, in 1993, the observed linear T -dependence of the penetration depth, $\lambda(T) - \lambda(0) \propto \Delta X_s(T) \propto T$ below 25 K in the ab -plane of high quality $\text{YBa}_2\text{Cu}_3\text{O}_{6.95}$ (YBCO) single crystals¹ gave rise to productive investigations of the order parameter of HTS's. Such linear variation of $\lambda(T)$ at low T has by now been observed not only in orthorhombic YBCO single crystals²⁻¹⁴ and films¹⁵⁻¹⁸, but also in tetragonal $\text{Bi}_2\text{Sr}_2\text{CaCu}_2\text{O}_8$ (BSCCO)¹⁹⁻²², $\text{Tl}_2\text{Ba}_2\text{CuO}_{6+\delta}$ (TBCO)^{23,24} and $\text{Tl}_2\text{Ba}_2\text{CaCu}_2\text{O}_{8-\delta}$ (TBCCO)¹⁰ single crystals. This temperature dependence is not in accord with a nearly isotropic superconducting gap and it is now considered to provide strong evidence for d -wave pairing in these materials²⁵⁻³⁵, in spite of the fact that the experimental data are not sensitive to the phase of the superconducting order parameter. Later research has shown that $\Delta\lambda_{ab}(T)$ could be linear at low T for models invoking the proximity effect between normal and superconducting layers³⁶ or assuming anisotropic s -wave pairing³⁷⁻³⁹. However, none of these theories can explain substantially different slopes of $\Delta\lambda_{ab}(T)$ at low T of YBCO samples grown by different methods⁴⁰ nor features, such as a bump^{9,11,16,41} or a plateau^{8,10,12}, observed in the intermediate temperature range $0.3T_c < T < 0.8T_c$. Models containing a mixed ($d + s$) symmetry of the order parameter⁴²⁻⁵⁶ hold some promise for a successful description of these experimental features, but this would require additional theoretical investigations.

Another important feature of the microwave response of HTS crystals is the linear variation with temperature of the surface resistance $R_s(T)$ in the ab -plane at

low temperatures. At frequencies of about 10 GHz and below the T -dependence of $R_s(T)$ in BSCCO, TBCO, and TBCCO single crystals is linear over the range $0 < T \lesssim T_c/2$ ^{19,21-23}. For YBCO crystals $\Delta R_s(T) \propto T$ for $T \lesssim T_c/3$ and $R_s(T)$ displays a broad peak and valley at higher temperatures^{4-14,57-61}. This peak can be understood in terms of a competition between an increase in the quasiparticle lifetime and a decrease in the quasiparticle density as the temperature is lowered. The fairly slow decrease in the quasiparticle density is indicative of a highly anisotropic or unconventional order parameter, resulting in a very small or vanishing energy gap, while the increase in the quasiparticle lifetime is attributed to the presence of inelastic scattering, which can be (i) due to the exchange of antiferromagnetic spin fluctuations⁶², which would naturally lead to d -wave pairing, or (ii) due to strong electron-phonon interaction⁶³⁻⁶⁵ within the anisotropic s -wave pairing model^{66,67}. Moreover, there have been suggestions of unconventional states for describing the charge carriers in the CuO planes like the marginal Fermi liquid^{68,69} and the Luttinger liquid^{70,71}. However, to fit the data of YBCO, the inelastic scattering rate has to decrease with temperature much faster than any of these microscopic models would predict. Further, the d -wave model, with point scatterers, does predict a finite low temperature and low frequency limit, which is independent of the concentration and the strength of the scattering centers⁷². Therefore, the latter model does not explain the very different values of the observed residual surface resistance $R_{\text{res}} \equiv R_s(T \rightarrow 0)$ on different samples. Furthermore, the value of this universal surface resistance is much lower than the R_{res} -values obtained from experiments. There is no microscopic theory which explains the linear temperature dependence of $\Delta R_s(T)$ up to $T_c/2$ in the crystals with non-orthorhombic structure and the shoulder of $R_s(T)$ observed on YBCO^{9,11} for $T > 40$ K.

In the absence of a generally accepted microscopic the-

ory a modified two-fluid model for calculating $Z_s(T)$ in HTS single crystals has been proposed independently in Refs.^{73,74} and then further developed in Refs.^{8,40,61,75}. Our phenomenological model has two essential features different from the well-known Gorter-Casimir model⁷⁶. The first is the introduction of the temperature dependence of the quasiparticle relaxation time $\tau(t)$ ($t \equiv T/T_c$) described by the Grüneisen formula (electron-phonon interaction), and the second feature is the unique density of superconducting electrons $n_s(t)$ which gives rise to a linear temperature dependence of the penetration depth in the ab -plane at low temperatures

$$\lambda^2(0)/\lambda^2(t) = n_s(t)/n \simeq n(1 - \alpha t), \quad (1)$$

where $n = n_s + n_n$ is the total carrier density, and α is a numerical parameter in our model.

The goal of this paper is to demonstrate the power of our model to describe the general and distinctive features of the surface impedance $Z_s(T)$ and the complex conductivity $\sigma_s(T)$ in the superconducting and normal states of different HTS crystals at various frequencies. The following section describes the systematization of the $Z_s(T)$ measurements, including the analysis which is used to extract $\sigma_s(T)$ from the measured values of $Z_s(T)$. Section III compares experimental data of $Z_s(T)$ and $\sigma_s(T)$ over the entire temperature range with calculations based on our modified two-fluid model. In the conclusion we compare the concepts of our model with results of microscopic theories. We hope that this will be a helpful guide for future investigations of microwave properties of HTS's from a microscopic point of view.

II. ANALYSIS OF EXPERIMENTAL RESULTS

A. Surface impedance

The surface impedance of HTS's, in terms of the complex conductivity $\sigma_s = \sigma_1 - i\sigma_2$, obeys the local equation (even at temperatures $T \ll T_c$):

$$Z_s = R_s + iX_s = \left(\frac{i\omega\mu_0}{\sigma_1 - i\sigma_2} \right)^{1/2}. \quad (2)$$

The impedance components are

$$R_s = \sqrt{\frac{\omega\mu_0(\varphi^{1/2} - 1)}{2\sigma_2\varphi}}, \quad (3)$$

$$X_s = \sqrt{\frac{\omega\mu_0(\varphi^{1/2} + 1)}{2\sigma_2\varphi}}, \quad (4)$$

where $\varphi = 1 + (\sigma_1/\sigma_2)^2$. It is obviously that $R_s < X_s$ for $T < T_c$.

For temperature $T < T_c$, if $\sigma_1 \ll \sigma_2$, Eqs. (3) and (4) reduce to

$$R_s \simeq \frac{(\omega\mu_0)^{1/2}\sigma_1}{2\sigma_2^{3/2}} = \frac{1}{2}\omega^2\mu_0^2\sigma_1\lambda^3, \\ X_s \simeq (\omega\mu_0/\sigma_2)^{1/2} = \omega\mu_0\lambda. \quad (5)$$

The components of the surface impedance are measurable quantities. The real part of the surface impedance, the surface resistance R_s , is proportional to the loss of the microwave power. It is caused by the presence of "normal" carriers. In the centimeter wavelength band, typical values of the surface resistance in the ab -plane of HTS single crystals are between 0.1 and 0.3 Ω above but near the transition temperature T_c . When T is decreased through T_c , the surface resistance abruptly drops, but does not seem to approach zero when $T \rightarrow 0$. In conventional superconductors, like Nb, $R_s(T)$ decreases exponentially with decreasing temperature below $T_c/2$, approaching a constant residual surface resistance R_{res} as $T \rightarrow 0$. R_{res} is due to the presence of various defects in the surface layer of the superconductor. Therefore, it is generally accepted that the lower the R_{res} , the better the sample quality. In high-quality HTS's there is no plateau in $R_s(T)$ at $T \ll T_c$. However, we shall extrapolate the value of $R_s(T)$ to $T = 0$ K and denote it by R_{res} . The origin of the residual surface resistance observed in HTS crystals remains unclear. It is known that R_{res} is strongly material and sample dependent and is approximately proportional to the square of the frequency. At present, very small values of $R_{\text{res}} \sim 20 \mu\Omega$ at frequencies ~ 10 GHz have been observed in YBCO single crystals^{9,14}.

The imaginary part of the surface impedance, the reactance X_s , is mainly determined by the superconducting carriers and is due to nondissipative energy stored in the surface layer of the superconductor.

In Table I⁷⁷ we summarized the main features of the temperature dependencies of the surface impedance of high-quality YBCO, BSCCO, TBCO, and TBCCO single crystals whose residual surface resistance in the ab -plane, R_{res} , at frequency of ~ 10 GHz is less than one milliohm, with $R_s(T_c)$ values of about 0.1 Ω . There is good reason to believe that the electrodynamic parameters of these crystals adequately relate to the intrinsic microscopic properties of the superconducting state of HTS.

To illustrate the data of Table I we show in Fig. 1, as an example, experimental data of $R_s(T)$ and $X_s(T)$ in ab -plane of BSCCO single crystal at 9.4 GHz²². In this figure $R_s(T) = X_s(T)$ for $T \geq T_c$, which corresponds to the normal skin-effect condition. Knowing $R_s(T_c) = \sqrt{\omega\mu_0\rho(T_c)}/2 \approx 0.12 \Omega$, we obtain the resistivity $\rho(T_c) \approx 40 \mu\Omega\cdot\text{cm}$. In the normal state, above T_c , the temperature dependence of $R_s(T) = X_s(T)$ is adequately described by the expression $2R_s^2(T)/\omega\mu_0 = \rho(T) = \rho_0 + bT$. For the BSCCO crystal in Fig. 1, $\rho_0 \approx 13 \mu\Omega\cdot\text{cm}$ and $b \approx 0.3 \mu\Omega\cdot\text{cm}/\text{K}$. The insets in Fig. 1 show $R_s(T)$ and $\lambda(T) = X_s(T)/\omega\mu_0$ for $T < 0.7T_c$, plotted on a linear scale. The extrapolation of the low-

TABLE I. Surface impedance $Z_s(T) = R_s(T) + iX_s(T)$ in the ab -plane of high- T_c single crystals at frequencies ~ 10 GHz

HTS	Superconducting state, $T < T_c$			Normal state $1.5 T_c > T \geq T_c$
	Low temperatures $4 \text{ K} < T \ll T_c$	Intermediate temperatures $T \sim T_c/2$	$T \rightarrow T_c$	
Orthorhombic structure YBCO $T_c \approx 92 \text{ K}$	$\Delta R_s(T) \propto T, \Delta X_s(T) \propto T$ at $T \lesssim T_c/4$; Essentially different slope of $\Delta\lambda(T) \propto T$ [1-14]	Broad peak in $R_s(T)$ at $25 < T < 45 \text{ K}$ [4-14] <u>Peculiarities:</u> 1. Shoulder [9,11] in $R_s(T)$ at $T > 40 \text{ K}$; 2. Bump [9] or plateau [8,10] on the curves of $X_s(T)$ at $50 < T < 80 \text{ K}$	Different slope of $\lambda(T)$ [3-14]	Normal skin-effect
Tetragonal structure BSCCO $T_c \approx 90 \text{ K}$ [19-22] TBCO $T_c \approx 80 \text{ K}$ [23,24] TBCCO $T_c \approx 110 \text{ K}$ [10,12]	$\Delta R_s(T) \propto T, \quad T \lesssim T_c/2$ $\Delta X_s(T) = \omega\mu_0\Delta\lambda(T) \propto T, \quad T \lesssim T_c/3$		Rapid growth of $R_s(T)$ and $X_s(T)$	$R(T) = X(T)$ = $\sqrt{\omega\mu_0\rho(T)/2}$ $\Delta\rho(T) \propto T$

temperature sections of these curves to $T = 0 \text{ K}$ yields estimates of $R_{\text{res}} = 0.5 \text{ m}\Omega$ and $\lambda_{ab}(0) = 2600 \text{ \AA}$ for this crystal.

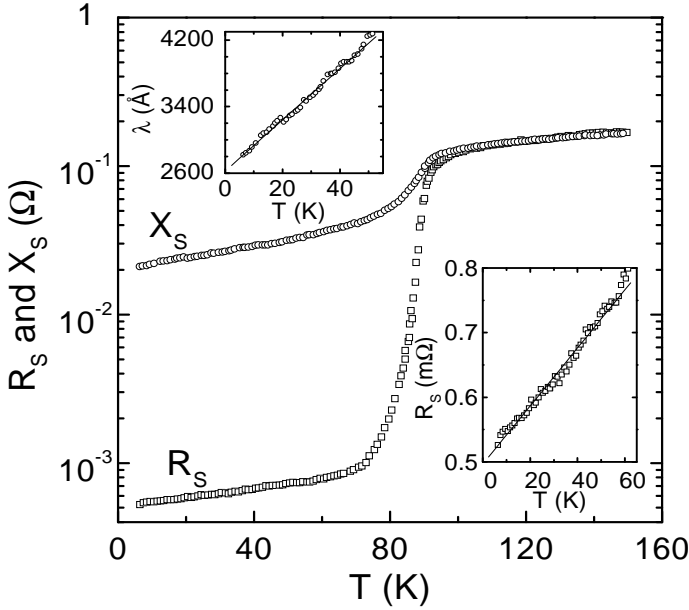


FIG. 1. Surface resistance $R_s(T)$ and reactance $X_s(T)$ in ab -plane of a BSCCO single crystal at 9.4 GHz. The insets show linear plots of $\lambda(T)$ and $R_s(T)$ at low temperatures.

The experimental $\Delta\lambda_{ab}(T)$ of YBCO, TBCO, and TBCCO crystals are also linear in the range $T < T_c/3$. It is important to notice the different slopes of the $\Delta\lambda(T) \propto T$ curves for $T \ll T_c$. In particular, in YBCO crystals, fabricated by different techniques, the slopes of $\Delta\lambda_{ab}(T)$ differs by almost one order of magnitude^{8,9,13}.

The reasons for such a discrepancy are still unclear.

At frequencies of about 10 GHz and below, the linear dependence $\Delta R_s(T) \propto T$ in BSCCO (Fig. 1), TBCCO, and TBCO single crystals may actually extend to temperatures of $\sim T_c/2$. This property, common for all HTS crystals with the tetragonal structure, is not characteristic of YBCO. As was noted previously, all microwave measurements on high-quality YBCO single crystals show a broad peak in the $R_s(T)$ curve centered near 30–40 K up to frequencies of ~ 10 GHz. The peak shifts to higher temperatures and diminishes in size as the frequency is increased. In YBCO crystals of higher quality the amplitude of the peak increases and $R_s(T)$ reaches its maximum at a lower temperature¹⁴.

The underlying origin of this YBCO feature has remained unclear. The simplest idea is that the absence of this peak in crystals with tetragonal structure might be caused by their “poor” quality, as is the case in YBCO doped with Zn^{2,4,58}. However, this deduction is probably incorrect because, (i), there is a sufficiently large set of experimental data indicating that $R_s(T)$ is a linear function of T for BSCCO, TBCO, and TBCCO, and (ii), the peak in $R_s(T)$ was also detected in such YBCO crystals^{7,10,60} with parameters R_{res} and $\rho(T_c)$ which would characterize the quality of these crystal as “poor” compared to those of, for example, TBCCO¹⁰ or BSCCO²¹. Results of the latter crystals are shown in Fig. 2. The more probable cause of the peak, however, is the presence of an additional component in the YBCO orthorhombic structure, namely CuO chains, which lead to a mixed ($d + s$) symmetry of the order parameter in YBCO. The electrons of the chains form an additional band, contributing to the observed T -dependence of $Z_s(T)$. This contribution seems to result in another

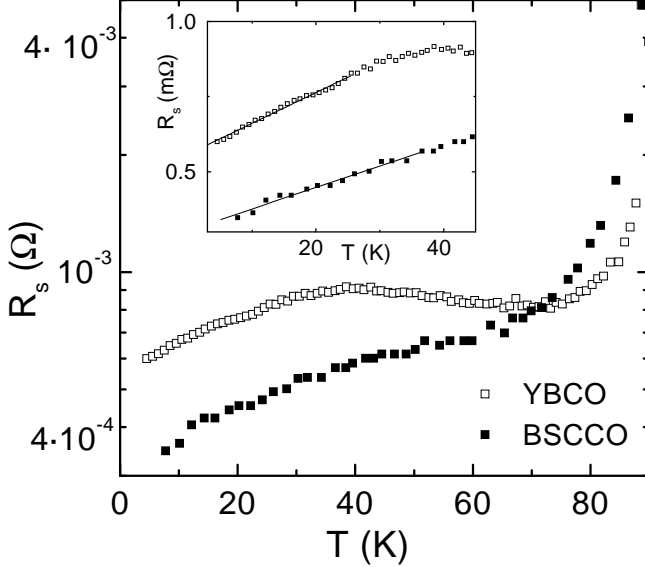


FIG. 2. Comparison of the temperature dependencies of surface resistance $R_s(T)$ of BSCCO and YBCO single crystals at 14.4 GHz. Experimental data are taken from Refs.²¹ (BSCCO at 14.4 GHz) and⁸ (YBCO at 9.4 GHz, scaled by ω^2 to 14.4 GHz). The inset shows the linear T -dependencies of R_s at low T for both materials, and a broad peak of $R_s(T)$ for YBCO.

distinctive feature of YBCO, namely a plateau or bump (see Table I) on the $\lambda_{ab}(T)$ curve, which has been observed in high-quality YBCO single crystals^{8–12} and films^{16,41}. However, recent measurements of $\Delta\lambda_{ab}(T)$ of YBCO crystals,¹⁴ grown in a high purity BaZrO₃ crucible, show no such features in the intermediate temperature range. The authors of Ref.¹⁴ argue that the disagreement with the results of Ref.⁹ arises from some problem connected with the surface of the crystal. The latter observation still lack a convincing explanation.

Finally, another feature in the T -dependence of the impedance of high-quality YBCO crystals was detected: a noticeable increase of $R_s(T)$ with increasing temperature (shoulder) at temperatures larger than the peak temperature at 30 K. It turns out that this shoulder was reproducible in the experiments^{9,11}. Similarly, an explanation of this observation is lacking.

B. Complex conductivity

Equations (2–4) allows us to express the real and imaginary parts of the complex conductivity $\sigma_s = \sigma_1 - i\sigma_2$ in terms of R_s and X_s :

$$\sigma_1 = \frac{2\omega\mu_0 R_s X_s}{(R_s^2 + X_s^2)^2}, \quad \sigma_2 = \frac{\omega\mu_0 (X_s^2 - R_s^2)}{(R_s^2 + X_s^2)^2}. \quad (6)$$

Above the superconducting transition temperature, the mean free path ℓ of current carriers is shorter than the

skin depth δ_n in the normal state (for $T \geq T_c$, $\ell \ll \delta_n$), which corresponds to the conditions of the normal skin effect. Equations (2–4), (6) also apply to the normal skin effect of HTS's, where $R_n(T) = X_n(T) = \sqrt{\omega\mu_0/2\sigma_n(T)}$ with $\sigma_n \equiv \sigma_1(T \geq T_c)$ and $\sigma_2 \ll \sigma_1$ at microwave frequencies.

The components $\sigma_1(T)$ and $\sigma_2(T)$ are not measured directly but derived from measurements of $R_s(T)$ and $X_s(T)$ using Eq. (6).

Low temperatures region ($T \ll T_c$)

When $R_s(T) \ll X_s(T)$, then Eq. (6) reduces to:

$$\sigma_1(T) = \frac{2\omega\mu_0 R_s(T)}{X_s^3(T)}, \quad \sigma_2(T) = \frac{\omega\mu_0}{X_s^2(T)}. \quad (7)$$

It then follows from Eq. (7), for low and intermediate temperatures that $\sigma_1/\sigma_2 = 2R_s/X_s \ll 1$. The increments of $\Delta\sigma_1(T)$ and $\Delta\sigma_2(T)$ depend on the increments of $\Delta R_s(T)$ and $\Delta X_s(T)$ relative to each other:

$$\Delta\sigma_1 \propto \left(\frac{\Delta R_s}{R_s} - 3 \frac{\Delta X_s}{X_s} \right), \quad \Delta\sigma_2 \propto - \frac{\Delta X_s}{X_s}. \quad (8)$$

It follows from Eq. (8) that the dominant changes of $\sigma_2(T)$ are determined mainly by the function $X_s(T) = \omega\mu_0\lambda(T)$, reflecting the T -dependence of the magnetic field penetration depth.

The T -dependence of the real part of the conductivity, $\sigma_1(T)$, is determined by the competition between the increments $\Delta R_s/R_s$ and $\Delta X_s/X_s$.

In conventional superconductors the quantity $X_s(T)$ ($\gg R_s$) is practically T -independent ($\Delta X_s \approx 0$) at temperatures $T \leq T_c/2$, and $R_s(T)$ decreases exponentially, approaching the residual surface resistance R_{res} as $T \rightarrow 0$. By subtracting R_{res} from the measured $R_s(T)$, we obtain, using Eqs. (7) and (8), the temperature dependence of $\sigma_1(T)$ predicted by the BCS theory: $\sigma_1 = 0$ at $T = 0$, AND for $T \leq T_c/2$, $\sigma_1(T)$ shows an exponentially slow growth with increasing temperature. Note that the smallest value of R_{res} detected in pure Nb is, at least, two order of magnitude smaller than the smallest value of R_{res} measured in YBCO. The extremely small values of the surface resistance in Eq. (8) indicate that the increment $\Delta\sigma_1(T)$, in classical superconductors is always positive ($\Delta\sigma_1(T) > 0$), at least in the temperature interval $T < 0.8T_c$, before the maximum of BCS coherence peak is reached.

For HTS single crystals the T -dependence of $\sigma_1(T)$ is radically different from that predicted by theories of the microwave response of conventional superconductors. In the T -range $T < T_c$ the increments of $\Delta R_s(T)$ and $\Delta X_s(T)$ in HTS's are not small, and, in addition, $\Delta X_s(T) \gg \Delta R_s(T)$. Although $R_s(T) < X_s(T)$, $\Delta R_s/R_s$ is not necessarily greater than $3\Delta X_s/X_s$ in Eq. (8) or positive at all temperatures. When that occurs, $\sigma_1(T)$ increases with decreasing temperature. The function $\sigma_1(T)$ is maximum at some $T = T_{\text{max}}$, and then $\sigma_1(T)$ becomes smaller with decreasing temperature. $\sigma_1(T)$ has a peak if the value of R_{res} is sufficiently small when for $T \rightarrow 0$:

$$R_{\text{res}} < \frac{X_s(0)}{3} \frac{\Delta R_s(T)}{\Delta X_s(T)}. \quad (9)$$

If inequality (9) is satisfied, T_{max} occurs at a finite temperature, while for R_{res} being equal to the right hand side of (9), T_{max} shifts to 0 K. If R_{res} is such that (9) is not satisfied, $\sigma_1(T)$ decreases at low temperatures as the temperature is increased, which is quite different from what is observed with conventional superconductors.

Thus, the shape of the $\sigma_1(T)$ for $T \ll T_c$ depends on the value of the residual surface resistance R_{res} , whose origin and accurate value are unknown. For this reason, the shapes of $\sigma_1(T)$ curves are not determined unambiguously for $T \leq T_c/2$, unlike the functions $R_s(T)$ and $X_s(T)$, which are directly measured in experiments.

If we linearly extrapolate $R_s(T)$ to $T = 0$ and attribute the resulting $R_s(0)$ to the residual surface resistance, $R_s(0) = R_{\text{res}}$, and then substitute the temperature dependent difference $R_s(T) - R_{\text{res}}$ into the numerator of the first expression of Eq. (7), the result is that the $\sigma_1(T)$ curve has a broad peak for HTS materials. Near $T = 0$, $\sigma_1(T)$ increases linearly with T from zero, reaches a maximum at T_{max} , and then decreases to $\sigma(T_c)$. This procedure, however, ignores the possibility of intrinsic residual losses. Therefore, some authors (see, e.g., Refs.^{14,21,59}) associate residual losses in HTS single crystals with a residual normal electron fluid. This implies that the source of the residual loss is in the bulk of the sample, although it is probably not intrinsic. If this contribution is excluded from the complex conductivity of the superconductor, one obtains $\sigma_1(T = 0) \rightarrow 0$, as can be seen in Fig. 3 from the measurements taken at 13.4, 22.7, and 75.3 GHz by the authors of Ref.¹⁴. The peak of $\sigma_1(T)$ shifts to higher temperatures and diminishes in size as the experimental frequency is increased. In YBCO single crystals the temperature T_{max} at which the maximum of σ_1 occurs is close to the temperature at which the peak of $R_s(T)$ occurs.

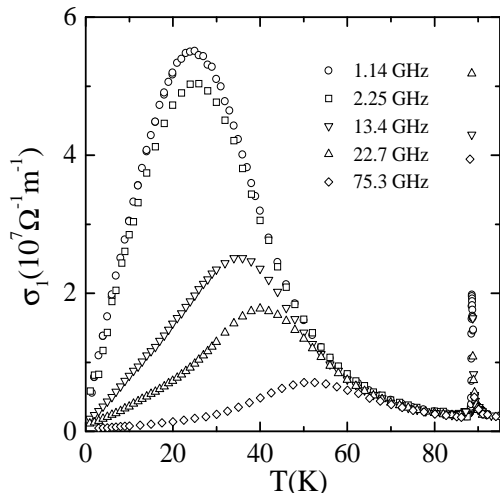


FIG. 3. Real part of the conductivity $\sigma_1(T)$ of YBCO single crystal at different frequencies¹⁴. The data were obtained courtesy of the Vancouver group (D. A. Bonn).

Finally, one may procure $\sigma_1(T)$ from measurements of $R_s(T)$ and $X_s(T)$ for $T > 0$ without any concern about R_{res} . In this case, $\sigma_1(0)$ is not determined uniquely. Whether $\sigma_1(T)$ has a peak or not depends on the validity of condition (9). The curves at 1 and 2 GHz in Fig. 3 have been obtained using Eq. (6) without subtracting any residual losses.

Temperatures close to T_c ($T \rightarrow T_c$)

Equations (7) and (8) do not apply near T_c . In this temperature range it is necessary to use the general local relationships (2–4), (6).

The conductivity $\sigma_2(T)$ in the ab -plane of HTS crystals abruptly drops to very small values in the normal state. The expression $(T_c/\sigma_2(0))d\sigma_2(T)/dT$ at $T = T_c$, defining the slope of $\lambda^2(0)/\lambda^2(T)$ at $T = T_c$, varies between -2 and -4 for different crystals.

The real part of the conductivity, $\sigma_1(T)$, does not show a coherence peak near $T = 0.85 T_c$, as predicted by BCS. Usually, the real part of the conductivity, $\sigma_1(T)$, of HTS single crystals has a narrow peak near T_c which increases with decreasing frequency^{21,23,24}. The width of the narrow peak of $\sigma_1(T)$ coincides with the width of the $R_s(T)$ transition at microwave frequencies. A possible explanation of the sharp peak just below T_c is inhomogeneous broadening of the superconducting transition^{78–80} or fluctuation effects^{24,81,82}.

III. MODIFIED TWO-FLUID MODEL

As was shown in Ref.⁶⁵, high T_c -values ($T_c \sim 100$ K), the temperature dependence of the resistivity, the frequency dependence of the momentum relaxation time, and other properties of the normal state in optimally doped HTS's are well described within the framework of the Fermi-liquid approach, including strong electron-phonon coupling (SC)⁶³. The SC model also explains some of the features of the superconducting state of HTS's. It follows from the Eliashberg theory that the distinctive component of superconductors with strong coupling is that the gap in the spectrum of electronic excitations is smeared. Strictly speaking, there is no gap, whatsoever, at $T \neq 0$ ^{83,84}. This leads to breaking of Cooper pairs, smearing of the peak in the density of states at $\hbar\omega = \Delta(T)$ due to inelastic scattering of electrons by thermally excited phonons, and suppression of coherence effects. As a result, the amplitude of the coherence peak decreases and, according to Refs.^{85,86}, virtually disappears at frequencies around 10 GHz if the electron-phonon coupling constant exceeds unity. Moreover, the mechanism of quasiparticle generation is radically different from that of the BCS model. The quasiparticles are generated without jumps across the energy gap and can be in states with all energies down to $\hbar\omega = 0$. These states can be classified as gapless, and the quasiparticles can be treated⁶⁵ as normal current carriers in the

two-fluid model. So it is not surprising that an important consequence of the SC model is the nonexponential behavior of $R_s(T)$ ⁸⁷ and $\lambda(T)$ ⁸⁸. Power-law temperature dependencies were also predicted by the two-fluid Gorter-Casimir (GC) model⁷⁶, and near T_c they proved to be quite close to calculations performed by the SC model. In particular, the curves of $\lambda^2(0)/\lambda^2(T)$, calculated by the SC model,^{89–92} proved to be fairly close to the function $n_s(t)/n = 1 - n_n(t)/n = 1 - t^4$ in the GC model. The slopes of these curves at $T = T_c$ are in agreement with those measured with different YBCO single crystals and are equal to^{4–3} or^{5,8,10} -4 . The experimental fact that there is no BCS coherence peak in the conductivity of HTS crystals, indicates the necessity of taking into account strong coupling effects near T_c and the feasibility of interpreting HTS properties at microwave frequencies in terms of a two-fluid model.

The complex conductivity σ_s is a basic property of superconductors. In accordance with GC model⁷⁶ the expressions for the components of $\sigma_s = \sigma_1 - i\sigma_2$ are:

$$\begin{aligned}\sigma_1 &= \frac{n_n e^2 \tau}{m} \left[\frac{1}{1 + (\omega\tau)^2} \right], \\ \sigma_2 &= \frac{n_s e^2}{m\omega} \left[1 + \frac{n_n}{n_s} \frac{(\omega\tau)^2}{1 + (\omega\tau)^2} \right].\end{aligned}\quad (10)$$

At temperatures $T \leq T_c$ the total carrier concentration is $n = n_s + n_n$, where $n_{s,n}$ are the fractions of superconducting and normal carrier densities (both have the same charge e and effective mass m). The real part of conductivity σ_1 is determined purely by the normal component, while both components, normal and superconducting, contribute to the imaginary part σ_2 . The relaxation time τ of normal carriers in the GC model is independent of temperature. This is acceptable if we assume that the behavior of normal carriers in superconductors is similar to that of normal carriers in normal metals at low temperatures. Scattering of electrons at very low temperatures is due to impurities and independent of the temperature. Therefore, the temperature dependence of the real part of the conductivity (10) in the GC model is determined entirely by the function $n_n(T)$ with $n_s(T) = n - n_n(T)$ only.

For sufficiently low frequencies $(\omega\tau)^2 \ll 1$ the expressions of the conductivity components of Eq. (10) transform into simple relations

$$\sigma_1 = \frac{e^2 \tau}{m} n_n, \quad \sigma_2 = \frac{e^2}{m\omega} n_s = \frac{1}{\mu_0 \omega \lambda^2}, \quad (11)$$

where $\lambda = \sqrt{m/\mu_0 n_s e^2}$ is the London penetration depth of a static magnetic field.

Penetration of alternating fields into superconductors is controlled by the frequency-dependent skin depth. Based on results of the complex conductivity (11), one obtains the complex skin depth δ_s by generalizing the corresponding expression for a normal conductor:

$$\delta_s = \frac{\sqrt{2}\lambda}{\sqrt{\omega\tau(n_n/n_s) - i}}. \quad (12)$$

With increasing angular frequency ω the skin depth $\text{Re}(\delta_s)$ decreases and, therefore, the London penetration depth λ gives the upper bound for the penetration of the electromagnetic field into a superconductor. In GC model the λ value diverges near T_c as $\lambda(t) = \lambda/[2\sqrt{1-t}]$ and the function $\sigma_2(t)/\sigma_2(0) = 4(1-t)$ tends linearly to zero at $T = T_c$ with a slope equal to -4 . At the same time, at $T = T_c$ the skin depth $\text{Re}(\delta_s)$, defined by Eq. (12), crosses over to the skin depth δ_n for a normal conductor.

A. Scattering and surface resistance of HTS single crystals

In conventional superconductivity one assumes that below T_c the mean free path does not vary with temperature. In a normal metal, at much higher temperatures than the corresponding T_c of a conventional superconductor, the electron scattering rate is proportional to T ⁹³. Since the transition temperatures of HTS's are much larger than those of conventional superconductors, it stands to reason that temperature will affect the electron scattering rate of the quasiparticles of HTS's below T_c , but be limited to a constant rate at low temperatures. Therefore, if a two-fluid model is to be successful in explaining transport properties of HTS's, then it is natural to include a temperature variation of τ into that model.

To obtain an expression for $\tau(T)$, we rely on the analogy between the 'normal fluid' component in the superconducting state and charge carriers in a normal metal. According to Mathissen's rule, the reciprocal relaxation time at temperatures below the Debye temperature Θ is

$$\frac{1}{\tau} = \frac{1}{\tau_{\text{imp}}} + \frac{1}{\tau_{\text{e-ph}}}. \quad (13)$$

The first term on the right is due to impurity scattering and is a constant of temperature, and the second is due to electron-phonon scattering and is proportional to T^5 .

From Eq. (13) we express $\tau(T)$ as

$$\frac{1}{\tau(t)} = \frac{1}{\tau(T_c)} \frac{\beta + t^5}{\beta + 1}, \quad (14)$$

where β is a numerical parameter: $\beta \approx \tau(T_c)/\tau(0)$, provided this ratio is much less than unity. It should be pointed out, however, that this approximation is not always satisfied.

Equation (14) corresponds to the low-temperature limit of the Bloch-Grüneisen formula, which includes impurity scattering and can be presented over a wide temperature range by the expression

$$\frac{1}{\tau(t)} = \frac{1}{\tau(T_c)} \frac{\beta + t^5 \mathcal{J}_5(\kappa/t)/\mathcal{J}_5(\kappa)}{\beta + 1}$$

$$\mathcal{J}_5(\kappa/t) = \int_0^{\kappa/t} \frac{z^5 e^z dz}{(e^z - 1)^2}, \quad (15)$$

where $\kappa = \Theta/T_c$. For $T < \Theta/10$ ($\kappa > 10t$), Eq. (15) approaches the form of Eq. (14). For $T > \Theta/5$ ($\kappa < 5t$), we obtain from Eq. (15) the linear T -dependence of $1/\tau(t) \propto t$. Examples of $1/\tau(t)$ for different parameters of β , κ , and $\tau(T_c)$ are shown in Fig. 4.

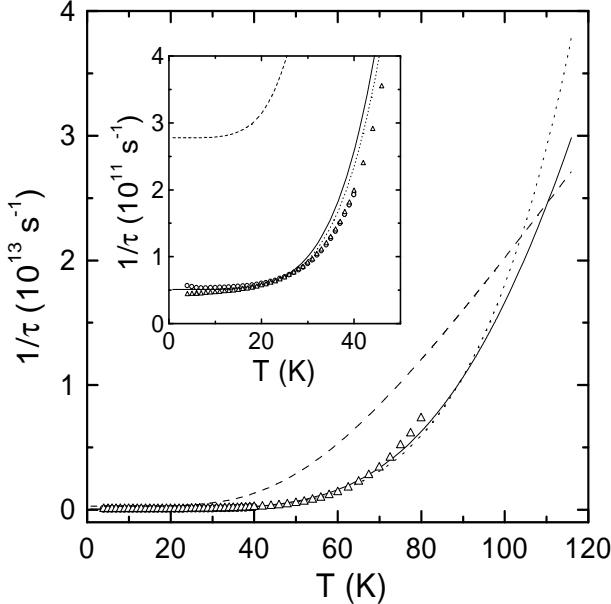


FIG. 4. Scattering rate of quasi-particles, calculated from Eq. (14), dotted line: $\beta = 0.005$, and Eq. (15), solid line: $\beta = 0.005$, $\kappa = 9$; dashed line: $\beta = 0.02$, $\kappa = 4$. The triangles are calculated from $1/\tau = [1 - \lambda^2(0)/\lambda^2(T)]/[\mu_o \sigma_1(T) \lambda^2(0)]$, with $\sigma_1(T)$ and $\lambda(T)$ at 1.14 GHz and $\lambda(0) = 1600$ Å in the ab -plane, with currents parallel to the a -direction of the YBCO crystal¹⁴. The inset shows the low temperature parts of the curves. The circles are from Fig. 8 of Ref.¹⁴.

For $\omega\tau(T_c) \ll 1$, which is normally satisfied at microwave frequencies, the parameter $\omega\tau(T_c)$ is obtained from measurements of $R_s(T_c)$ and $X_s(0)$:

$$\omega\tau(T_c) = \frac{X_s^2(0)}{2R_s^2(T_c)} = \frac{\sigma_1(T_c)}{\sigma_2(0)}. \quad (16)$$

At frequencies ~ 10 GHz, the value $\omega\tau$ of the best HTS crystals is of the order of 10^{-3} at $T = T_c$ and remains less than unity at all temperatures $T < T_c$, as will be discussed below. Therefore, the expressions of the conductivity components in Eq. (10) in the two-fluid model turn into the simple form (11).

All experimental data of $R_s(T)$ of high-quality HTS single crystals can be elucidated by our two-fluid model with $\tau(T)$ given by Eqs. (14) or (15).

Measurements of $R_s(T)$ of YBCO single crystals at frequencies of order or less than 10 GHz are analyzed

first. Values of $\sigma_2(T)/\sigma_2(0) = \lambda^2(0)/\lambda^2(T) = n_s(T)/n$, measured in the same experiments, and $\sigma_1(T)/\sigma(T_c)$ obtained from Eq. (11) are substituted into the Eq. (3). Use is made of the relation $n_n(T)/n = 1 - \sigma_2(T)/\sigma_2(0)$, which is obtained from the experimental data, and $\tau(T)$, employing Eqs. (14) or (15).

Setting $\beta = 0.005$ and $\kappa = 9$ in Eq. (15) and taking the experimental values $\sigma_2(T)/\sigma_2(0)$ from Fig. 11 (see below) and $\omega\tau(T_c) = 7.5 \times 10^{-4}$ at 1.14 GHz we find from Eqs. (11) and (3) the T -dependencies of $R_s(T)$, shown by the curves in Fig. 5. These curves match the data of Ref.¹⁴ over the entire temperature range. The same result is obtained using Eq. (14) instead of Eq. (15), with $\beta = 0.005$. For at $\kappa \gg 1$ and $T \lesssim T_c$, Eqs. (14) and (15) are identical.

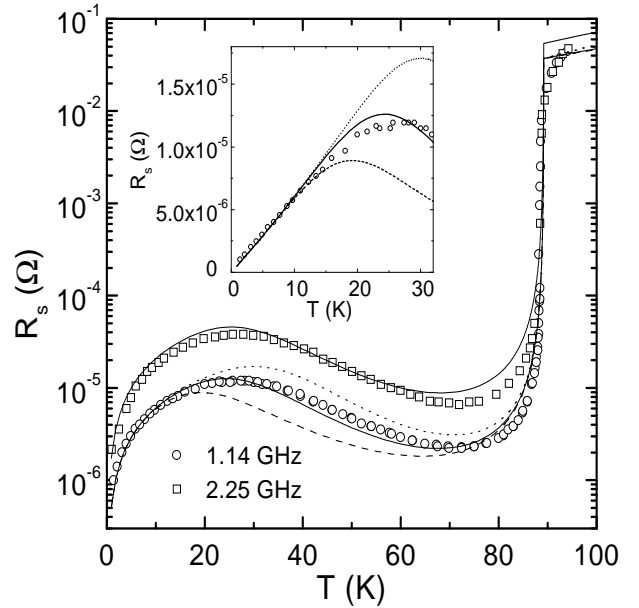


FIG. 5. Experimental $R_s(T)$ data of YBCO single crystal¹⁴ at 1.14 GHz (circles) and 2.25 GHz (squares). Solid curves are calculations using Eqs. (3), (11) and (14). The dashed curves are calculated at 1.14 GHz with the term t^5 replaced by t^4 in the numerator of Eq. (14), the dotted curves with t^6 . The inset shows a linear plot of $R_s(T)$ at low temperatures at 1.14 GHz.

From Eqs. (5) and (11) it follows that for $\alpha t \ll 1$ [see Eq. (1)] a rough estimate of the temperature t_m at which $R_s(T)$ is maximum is obtained from the relation $\beta \simeq 4t_m^5$. The value of $\tau(0)$ is found from the slopes dR_s/dT and $d\lambda/dT$ of the experimental data of $R_s(T)$ and $\lambda(T)$ as $T \rightarrow 0$ [$\omega\tau(0) < 1$]:

$$\omega\tau(0) = \frac{1}{\mu_o \omega} \frac{dR_s}{d\lambda}. \quad (17)$$

With Eq. (16) and (17) the parameter $\beta \approx \tau(T_c)/\tau(0)$ is determined from the surface impedance data. As β increases the maximum and minimum of $R_s(T)$ change into an inflection point with a horizontal tangent and

for larger β values the maximum of $R_s(T)$ disappears completely⁷⁴.

The linear T -increase of $R_s(T)$ at low temperatures (inset in Fig. 5) is a direct consequence of the linear change of $\lambda(T)$ near $T = 0$, proportional to the coefficient α in Eq. (1), and due to a constant scattering rate at low temperatures, as shown in Fig. 4.

The dashed and dotted curves in Fig. 5, are calculated $R_s(T)$ values at 1.14 GHz, with t^5 replaced by t^4 (dashed curve) and by t^6 (dotted curve) in Eq. (14). The best fit of the experimental data is $1/\tau(t) \propto t^5$. Moreover, Eq. (15) enables us to incorporate the shoulder of $R_s(T)$ obtained with YBCO single crystals in Refs.^{9,11}. This is shown in Fig. 6, which contains measurements (squares) of $R_s(T)$ at 10 GHz taken from Ref.⁹, and calculations (solid line) of $R_s(T)$ using Eqs. (11) and (3) with $\omega\tau(T_c) = 4 \times 10^{-3}$, $\sigma_2(T)/\sigma_2(0)$ obtained from the same experimental data⁹, $\beta = 0.02$ and $\kappa = 4$ in Eq. (15)⁸.

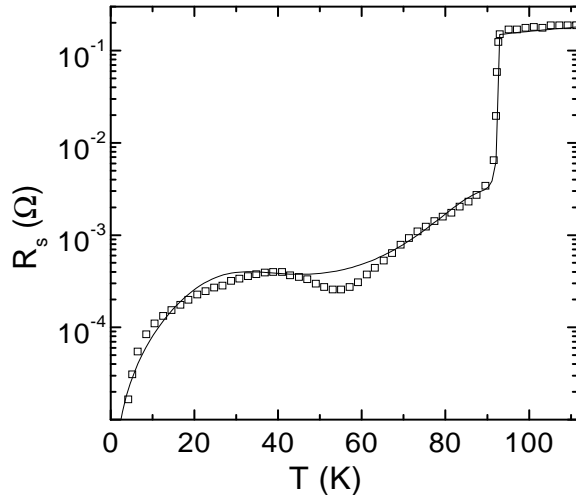


FIG. 6. Comparison between calculated (solid line) and measured (squares) surface resistance $R_s(T)$ of YBCO single crystal at 10 GHz. Experimental data are from Ref.⁹.

The calculated curves in Figs. 5 and 6 are very close to the experimental data and display the common and unique features of $R_s(T)$ for $T < T_c$ and $\omega\tau < 1$ of high-quality YBCO single crystals fabricated by different methods, namely: (i) the linear temperature dependence of surface resistance, $\Delta R_s(T) \propto T$, caused by the linear variation of $\Delta X_s(T) \propto \Delta \lambda_{ab}(T) \propto T$ at temperatures $T \ll T_c$, and by $\tau(T) \rightarrow \text{const}$ at low temperatures; (ii) the broad peak of $R_s(T)$ in the intermediate temperature range due to the rapid decrease of the relaxation time $\tau(T) \propto T^{-5}$, with increasing temperature; and (iii) the increase in $R_s(T)$ in the range $T_c/2 < T < T_c$ (Fig. 6) caused by the crossover from T^{-5} to T^{-1} of $\tau(T)$ in Eq. (15), which occurs in Fig. 6 at a lower temperature than in Fig. 5. The behavior of $1/\tau(T)$ for these two YBCO crystals is shown in Fig. 4.

Up to this point, our analysis has not taken into ac-

count the residual surface resistance R_{res} of the samples. In the YBCO crystals whose data are plotted in Figs. 5 and 6, scaled to the same frequency of 10 GHz, the resistance $R_{\text{res}} < 50 \mu\Omega$. $R_{\text{res}}/R(T_c) < 10^{-3}$ is so small that R_{res} was neglected even at $T \ll T_c$. In most HTS crystals which were investigated, however, $R_{\text{res}}/R(T_c) > 10^{-3}$ (see, e.g., Figs. 1 and 2). Therefore, it is important that R_{res} is added to the calculated $R_s(T)$ values when comparing the latter with the experimental data.

Figure 7 compares the measured $R_s(T)$ and $X_s(T)$ of BSCCO, plotted in Fig. 1, with calculations obtained from Eqs. (3) and (4). In this case, we have added to the calculated values of $R_s(T)$ a constant $R_{\text{res}} = 0.5 \text{ m}\Omega$. The calculation is based on measurements of $\sigma_2(T)/\sigma_2(0)$ obtained in the same experiment and plotted in the inset to Fig. 13 (see below), with parameter $\omega\tau(T_c) = 0.9 \times 10^{-2}$, $\beta = 2$ and $\kappa = 3$ in Eq. (15). It is clear that the agreement between the calculated and experimental curves is good throughout the temperature interval $5 \leq T \leq 120 \text{ K}$.

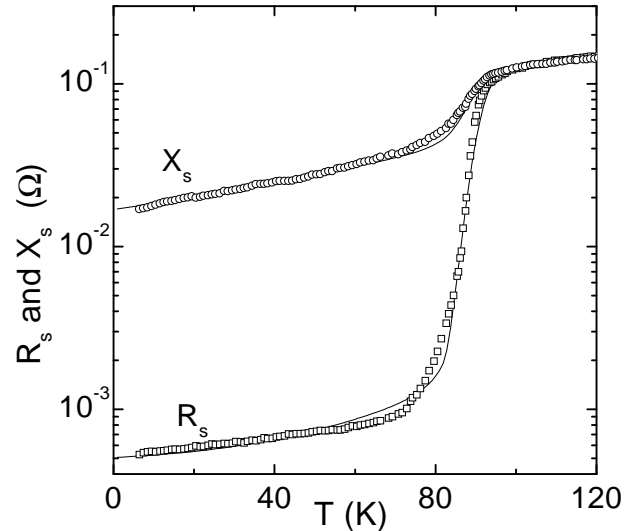


FIG. 7. Comparison between calculated (solid lines) and measured surface impedance (symbols) of BSCCO single crystal (see Fig. 1). A constant $R_{\text{res}} = 0.5 \text{ m}\Omega$ is added to the values of $R_s(T)$, obtained from Eq. (3).

Another reason for including R_{res} is that the ratio $R_{\text{res}}/R(T_c) \propto \omega^{3/2}$. Fig. 8 is based on the experimental data of BSCCO single crystal measured in Ref.²¹ at three frequencies: 14.4 GHz ($\omega\tau(T_c) = 0.7 \times 10^{-2}$), 24.6 GHz, and 34.7 GHz. The solid curves are calculations at these frequencies obtained from Eqs. (11) and (3) using $\tau(T)$ from Eq. (15) with $\beta = 0.1$ and $\kappa = 4$. The comparison procedure is different from that discussed above for YBCO crystals since $R_{\text{res}} \propto \omega^2$ is added to the calculated $R_s(T)$ values. The inset of Fig. 8 shows a linear plot of the measured and calculated surface resistance at low temperatures. We emphasize that at temperatures below $T_c/2$ the value of $\Delta R_s(T)$ changes proportional to T .

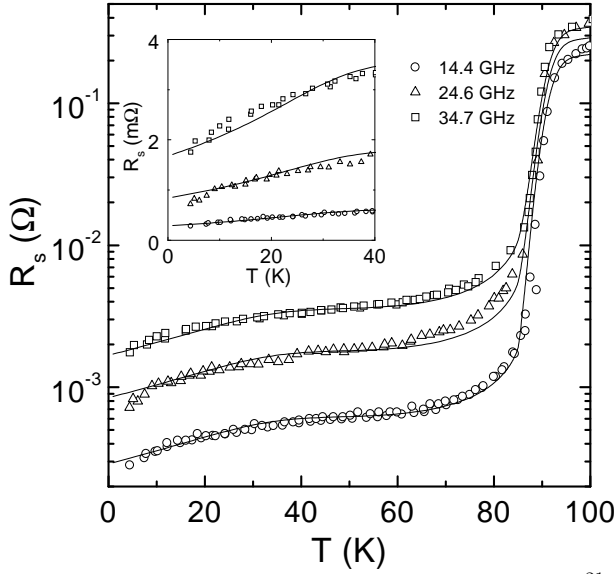


FIG. 8. Experimental data of BSCCO single crystal²¹ at various frequencies: 14.4 GHz, 24.6 GHz, and 34.7 GHz. The solid curves are the calculated $[R_s(T) + R_{\text{res}}]$ -functions, with R_{res} values of 0.29, 0.85 and 1.7 m Ω , respectively. The inset shows the linear temperature dependencies of the surface resistance at low temperatures.

In the millimeter and shorter wavelength bands, the condition $\omega\tau < 1$ may not be satisfied in the superconducting state of the purest HTS single crystals due to the fast growth of $\tau(T)$ with decreasing $T < T_c$. Therefore, it is natural not only to take R_{res} into account in analyzing the experimental data of $Z_s(T)$ and $\sigma_s(T)$ but also the more general Eq. (10) of the two-fluid model should replace Eq. (11). The $R_s(T)$ data of Ref.¹⁴ at frequencies of 13.4, 22.7, and 75.3 GHz, are shown in Fig. 9 with the calculated $R_s(T)$ values (obtained on the same YBCO crystal as was used in Fig. 5). We used $\tau(T_c)/\tau(0) \approx \beta = 5 \times 10^{-3}$ in Eq. (14) for all curves

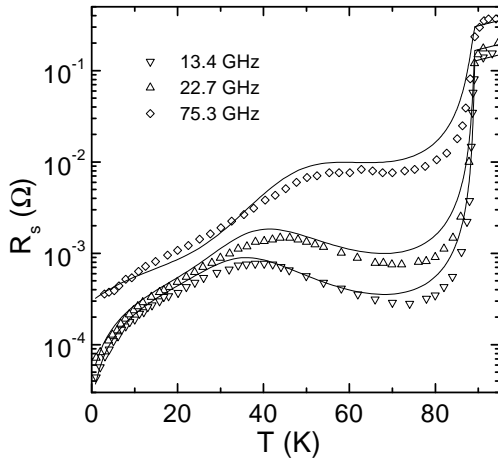


FIG. 9. Comparison between calculated (lines) and measured¹⁴ (symbols) surface resistance $R_s(T)$ of YBCO single crystal at 13.4, 22.7 and 75.3 GHz. We assumed $R_{\text{res}} = 0.3$ m Ω for 75.3 GHz, zero for the other frequencies.

shown in Fig. 9 (same as previously used in Fig. 5), and added $R_{\text{res}} = 0.3$ m Ω to $R_s(T)$ [Eq. (3)] at 75.3 GHz only. The conductivity components $\sigma_1(T)$ and $\sigma_2(T)$ which are contained in Eq. (3) are obtained from the experimental data of $\sigma_2(T)/\sigma_2(0)$ at 1.14 GHz,¹⁴ (shown in Fig. 11), and from Eq. (10).

Figure 10 shows another example. The experimental $R_s(T)$ data (squares) of TBCO single crystal ($T_c = 78.5$ K)²³ are compared with calculations based on Eqs. (3), (10), and (15). The curve representing the theoretical $R_s(T) + R_{\text{res}}$ was plotted using $\beta = 0.1$, $\kappa = 5.5$, $\omega\tau(T_c) = 1.7 \times 10^{-2}$, $R_{\text{res}} = 0.8$ m Ω , and with $\sigma_2(T)/\sigma_2(0)$, shown in the inset (circles) of Fig. 10.

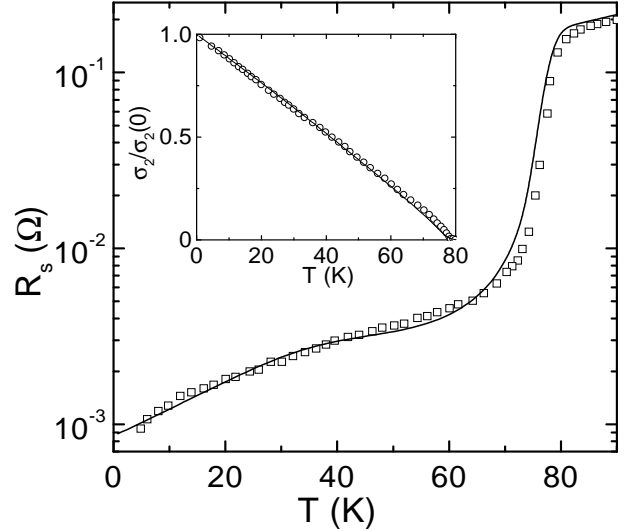


FIG. 10. Surface resistance $R_s(T)$ of a TBCO single crystal at 24.8 GHz taken from Ref.²³ Solid curve is the calculated $[R_s(T) + R_{\text{res}}]$ -function with $R_{\text{res}} = 0.8$ m Ω . The inset shows measured²³ (circles) and calculated results of $\sigma_2(T)/\sigma_2(0)$ (solid line), using Eq. (18) with $\alpha = 0.9$.

B. Temperature dependence of the superconducting electron density

Our phenomenological model would be incomplete if simple formulas were not available that describe correctly the measurements of $\Delta\lambda_{ab}(T)$. Figures 10 (inset), 11 and 12 show $\sigma_2(T)/\sigma_2(0) = \lambda^2(0)/\lambda^2(T) = n_s(T)/n$ in the ab -plane of TBCO, YBCO, and BSCCO single crystals from Refs.^{23,14} and²¹, respectively. All of these quantities change linearly with temperature at low-temperatures and can be approximated by the function⁷³

$$n_s/n = (1 - t)^\alpha, \quad (18)$$

where α is a numerical parameter. For $t \ll 1$, Eq. (1) follows from Eq. (18). For the cited experiments, the values of α fall into the range $0.4 < \alpha \leq 0.9$. Near T_c we obtain $\lambda(t) \propto n_s(t)^{-1/2} \propto (1 - t)^{-\alpha/2}$, which is also

in fairly good agreement with experimental data. However, equation (18) yields an infinite value of derivative $d\sigma_2(t)/dt \propto (1-t)^{\alpha-1}$ at $t=1$ for $\alpha < 1$.

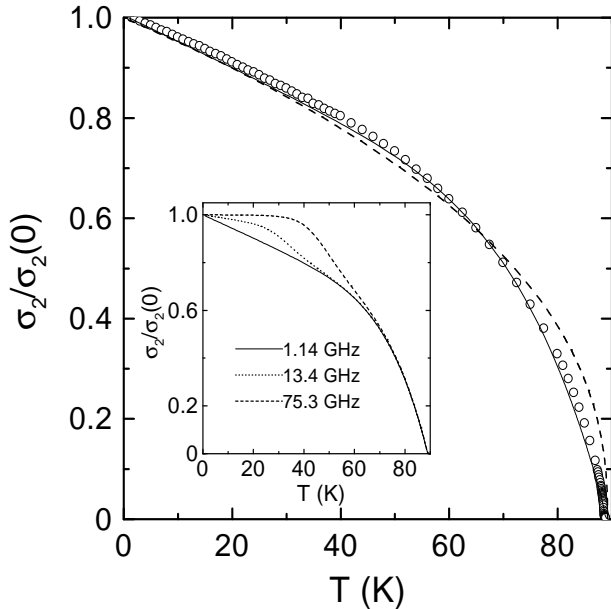


FIG. 11. Plots of Eq. (18) (dashed line, $\alpha = 0.42$) and Eq. (19) (solid line, $\alpha = 0.47$), showing the fit to the empirical $\sigma_2(T)/\sigma_2(0)$. The experimental data (circles) are from Ref.¹⁴ at 1.14 GHz. The inset shows the temperature dependencies of $\sigma_2(T)/\sigma_2(0)$ at various frequencies, calculated from Eqs. (10), (19) and (14).

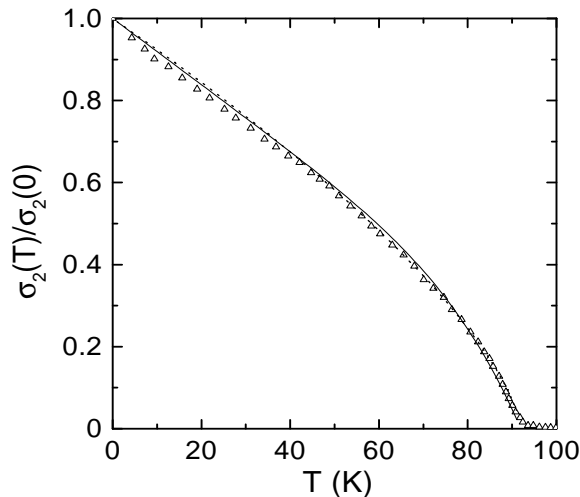


FIG. 12. Comparison between calculated (solid curve: Eq. (19), $\alpha = 0.74$; and, dotted line: Eq. (18), $\alpha = 0.7$) and measured²¹ (symbols) of $\sigma_2(T)/\sigma_2(0)$ values of BSCCO single crystal⁷⁵.

An approximation for $n_s(t)/n$ close to Eq. (18) was proposed in Ref.⁷⁵:

$$n_s/n = 1 - \alpha t - (1 - \alpha)t^6 \quad (19)$$

and is shown by solid lines in Figs. 11 and 12. Equa-

tion (19) insures that the slope at T_c of $\lambda^2(0)/\lambda^2(t)|_{T_c} = (5\alpha - 6)$ is finite and negative for $\alpha < 1.2$.

The above functions for $n_s(t)$, however, in their simplest forms (18) and (19), cannot account for all features in $\lambda^2(0)/\lambda^2(T)$ detected recently in YBCO crystals (see Table I) in the intermediate temperature range⁸⁻¹¹. Moreover, the slope of these curves at $T \ll T_c$ requires that $\alpha > 1$ in Eq. (18), which would lead to zero slope of the $\sigma_2(T)/\sigma_2(0)$ curve at $T = T_c$. Therefore we have added an additional empirical term to the right-hand side of Eq. (18) without violating the condition of particle conservation, $n_s + n_n = n$,

$$n_s/n = (1-t)^\alpha(1-\delta) + \delta(1-t^{4/\delta}), \quad (20)$$

where $0 < \delta < 1$ is the weight factor⁸. For $\delta \ll 1$ and $\alpha > 1$ the dominant contribution to $\sigma_2(T)$ throughout the relevant temperature range is still due to the first term on the right of Eq. (20), while the second is responsible for the finite slope of $\sigma_2(T)/\sigma_2(0)$ at $T = T_c$, equal to -4 , in accordance with the GC model. As δ increases, the second term on the right side of Eq. (20) becomes more essential. The experimental curve of $\sigma_2(T)/\sigma_2(0)$, derived from $R_s(T)$ and $X_s(T)$ measurements of YBCO crystal in Ref.⁸, is properly described by Eq. (20) with $\delta = 0.5$ and $\alpha = 5.5$ (Fig. 13). This calculation reflects the characteristic features of the experimental data, namely, the linear section of n_s and the positive second derivative ($\alpha > 1$) in the low-temperature region, the plateau in the intermediate temperature range, and the correct value of the slope near T_c .

Using Eq. (20) with $\alpha = 2$ and $\delta = 0.2$, one can also describe the T -dependence of $\sigma_2(T)$ of BSCCO crystals (Figs. 1 and 7), plotted in the inset to Fig. 13.

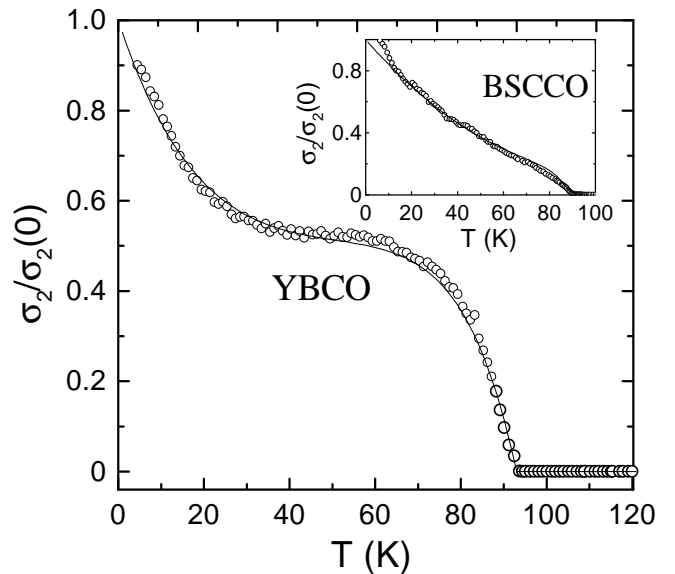


FIG. 13. Comparison between calculated (solid line) and measured (circles) values of $\sigma_2(T)/\sigma_2(0)$ of YBCO single crystal⁸. The inset shows the measured and calculated values, using Eq. (20) for the temperature dependencies of $\sigma_2(T)/\sigma_2(0)$ of the BSCCO crystal, shown in Fig. 1.

C. Real part of conductivity

Since the measurements and calculations of $R_s(T)$, $X_s(T)$, and $\sigma_2(T)$ are in good agreement and consistent with $\sigma_1(T)$ in the range $T < T_c$, it is proposed that the modified two-fluid model is a powerful tool for describing the electrodynamic properties of HTS's. The only feature that has not been investigated by this model is the behavior of $Z_s(T)$ and $\sigma_s(T)$ in the temperature range near T_c . A spectacular display is the narrow peak in the real part of the conductivity (see Fig. 3).

$\sigma_1(T)$ of YBCO crystals, obtained from measurements at 1.14 GHz¹⁴, is plotted (circles) in Figs. 3 and 14.

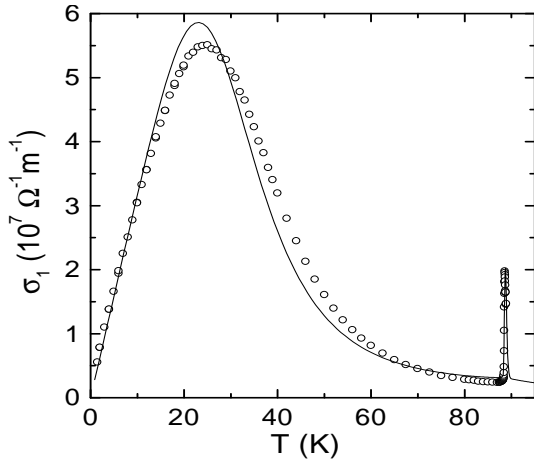


FIG. 14. Comparison of the experimental T -dependence of $\sigma_1(T)$ (open circles in Fig. 3) of YBCO single crystal at 1.14 GHz (Ref.¹⁴) with that calculated using the modified two-fluid model (solid line), taking into account the inhomogeneous broadening of the superconducting transition ($\delta T_c = 0.4$ K in Eq. (21)).

The narrow peak near T_c can be described by an effective medium model^{80,94} which takes into account inhomogeneous broadening of the superconducting transition. Assume that different regions of a given specimen experience transitions to the superconducting state at different temperatures within the T -range δT_c . If the dimension of each of these regions is smaller than the magnetic field penetration depth (microscopic-scale disorder), the distribution of the microwave currents over the sample is uniform, and the calculation of the effective impedance Z_{eff} of the sample reduces to two operations: first, the impedances Z_s of all regions in the specimen (with different T_c) that are connected in series along a current path are added, and, second, averaging over the sample volume is performed. As a result, we obtain

$$Z_s^{\text{eff}}(T) = R_s^{\text{eff}}(T) + iX_s^{\text{eff}}(T) = \int_{\delta T_c} Z_s(T, T_c) f(T_c) dT_c, \quad (21)$$

where the distribution function $f(T_c)$ is such that the fraction of the sample volume with critical temperatures in the range $T_c < T < T_c + dT_c$ equals $f(T_c)dT_c$. In the simplest case $f(T_c)$ is a Gaussian function. In the experiments of Ref.¹⁴, the width of the superconducting resistive transition was approximately 0.4 K, which we equate to the width of the Gaussian distribution $f(T_c)$. Using the general relations (6), with the effective impedance components obtained from Eq. (21), $\sigma_1^{\text{eff}}(T)$ is calculated near T_c and is plotted with the experimental data in Fig. 14 for YBCO¹⁴. The overall agreement is good.

In the framework of the discussed approach, $\sigma_1^{\text{eff}}(T)$ displays a narrow peak at $T^* = T_c - \delta T_c$. It is easy to check that the relative peak amplitude is approximately equal to

$$\frac{\sigma_1(T^*) - \sigma(T_c)}{\sigma(T_c)} \approx \begin{cases} \gamma, & \text{if } \gamma > 1 \\ \gamma^2, & \text{if } \gamma < 0.1 \end{cases}, \quad (22)$$

where $\gamma = \delta T_c / [T_c \omega \tau(T_c)]$, implying, the narrower the superconducting resistive transition, the smaller the peak amplitude. Usually, experiments yield $\gamma > 1$ (e.g., the data of Ref.¹⁴ gives $\gamma \simeq 7$ at 1.14 GHz) and, therefore, the peak amplitude should be inversely proportional to frequency.

We applied the above procedure to other specimens to incorporate corrections into the calculations of the $\sigma_1(T)$ curves, caused by inhomogeneous broadening of the superconducting transition. We adjusted the previous calculations of $R_s(T)$ (Figs. 7, 8, and 10) and $\sigma_2(T)$ (Figs. 10, 12, and inset to Fig. 13) by substituting the resulting $Z_s^{\text{eff}}(T)$ into the general equation (6) for the conductivity σ_1 . The resulting curves for BSCCO and TBCO are shown in Figs. 15–17.

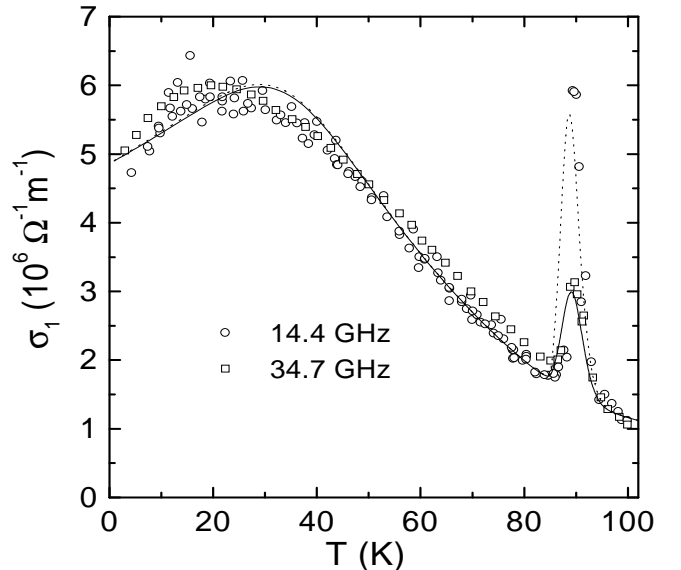


FIG. 15. Experimental data of $\sigma_1(T)$ at 14.4 and 34.7 GHz of BSCCO single crystal²¹ and calculations of $\sigma_1(T)$ using Eqs. (14), (3), (21) and (10), taking into account sample inhomogeneities ($\delta T_c = 2$ K).

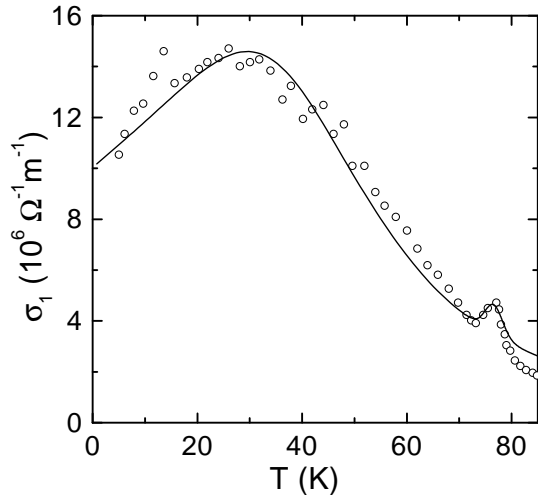


FIG. 16. Comparison of the T -dependence of the experimental $\sigma_1(T)$ (open circles) of TBCO single crystal at 24.8 GHz (Ref.²³) with that calculated using the modified two-fluid model (solid line), taking into account the inhomogeneous broadening of the superconducting transition ($\delta T_c = 2.5$ K in Eq. (21)).

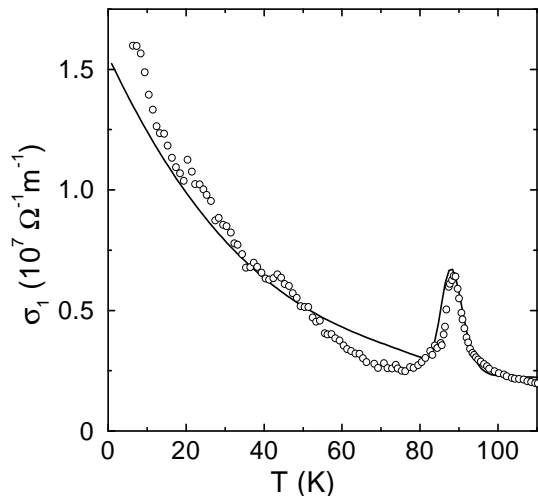


FIG. 17. Conductivity $\sigma_1(T)$ of BSCCO single crystal at 9.4 GHz, extracted from the surface impedance measurements of Fig. 1, and calculation based on the modified two-fluid model, which takes into account the inhomogeneous broadening of the superconducting transition ($\delta T_c = 4.5$ K). $\sigma_1(T)$ does not have a broad peak at low temperatures in this particular case.

IV. CONCLUSION

We have presented a summary of measurements of the surface impedance $Z_s(T) = R_s(T) + iX_s(T)$ of high-quality YBCO, BSCCO, TBCO and TBCCO crystals in the superconducting and normal states (Table I). For frequencies $\lesssim 10$ GHz the common features of all these materials are the linear temperature dependence of surface resistance, $\Delta R_s(T) \propto T$, of the surface reactance,

$\Delta X_s(T) \propto \Delta \lambda_{ab}(T) \propto T$, at temperatures $T \ll T_c$, their rapid growth as $T \rightarrow T_c$, and their behavior in the normal state corresponding to a linear T -dependence of $\Delta \rho_{ab}(T)$, with $R_s(T) = X_s(T) = \sqrt{\omega \mu_0 \rho(T)/2}$. There are differences between the T -dependence of $Z_s(T)$ of BSCCO, TBCCO or TBCO single crystals, with tetragonal lattices, compared to YBCO crystals, with an orthorhombic lattice. The linear resistivity region of the tetragonal materials extends to near $T_c/2$, while for YBCO the linear region terminates near or below $T < T_c/3$. At higher temperature, $R_s(T)$ of YBCO has a broad peak. In addition, the $\lambda_{ab}(T)$ curves of some YBCO single crystals have unusual features in the intermediate temperature range.

We describe all of the above features of $Z_s(T)$ and $\sigma_s(T) = \sigma_1(T) - i\sigma_2(T) = i\omega\mu_0/Z_s^2(T)$ of high-quality HTS crystals by generalizing the well-known GC two-fluid model:

(i) we introduce a temperature dependence of the relaxation time of the quasiparticles in accordance with the Bloch-Grüneisen law. We find that the $R_s(T)$ curves in different HTS crystals are well described using Eqs. (14) or (15) for $1/\tau(T)$. In the latter equation there is only one fitting parameter, $\kappa = \Theta/T_c$, while the other parameter $\beta = \tau(T_c)/\tau(0) \ll 1$ can be estimated directly from the experimental data with the help of Eqs. (16) and (17). The absence of the broad peak of $R_s(T)$ in tetragonal HTS single crystals is due to a less rapid increase of $\tau(T)$ with decreasing temperature. In other words, the value of β is smaller for YBCO crystals than for BSCCO, TBCO or TBCCO. For the latter crystals the residual losses R_{res} are usually large and they have to be taken into account. (ii) we replace the well-known temperature dependence of the density of superconducting carriers in the GC model, $n_s = n(1 - t^4)$, by one of the functions proposed by Eqs. (18), (19) or (20). All of these functions change linearly with temperature at $t \ll 1$ (see Eq. (1)). This permits one to extract the common and distinctive features of $X_s(T)$ and $\sigma_2(T)$ from different HTS crystals.

It also follows from the equations of the modified two-fluid model, that at low temperatures, $t \ll 1$, and low frequencies ($\omega\tau(0) < 1$), all curves of $Z_s(T)$ and $\sigma_s(T)$ have linear regions: $\sigma_1 \propto \alpha t/\beta$, since $n_n/n \approx \alpha t$ and $\tau \approx \tau(0) \approx \tau(T_c)/\beta$. Furthermore, $\Delta\sigma_2 \propto -\alpha t$. Then, in accordance with Eq. (5), $R_s \propto \alpha t/\beta$ and $\Delta X_s \propto \Delta\lambda \propto \alpha t/2$. As the temperature increases, the curve of $\sigma_1(t)$ passes through a maximum at $t \lesssim 0.5$ if the inequality (9) is valid. This peak is due to superposition of two competing effects, namely, the decrease in the number of normal carriers as the temperature decreases, for $t < 1$, and the increase in the relaxation time, which saturates at $t \sim \beta^{1/5}$, at which point the impurity scattering starts to dominate. The features in the $X_s(T)$ and $\sigma_2(T)$ curves for YBCO single crystals in the intermediate temperature range (plateau⁸ or bump⁹) can also be described within the framework of our modified two-fluid model, if we take into account the modification of $n_s(t)$, described by Eq. (20) with $0 < \delta \leq 0.5$. The nar-

row peak in the real part of the conductivity $\sigma_1(T)$, near T_c , in HTS single crystals can be explained in terms of an effective medium model, taking into account strong electron-phonon coupling of the quasiparticles and inhomogeneous broadening of the superconducting transition.

It is natural to compare the tenets of our phenomenological model with the results of microscopic theories. As was shown in Refs.⁴⁰ and⁶¹, the simple formula (1), which defines the linear low temperature dependence of the magnetic field penetration depth in the ab -plane of HTS crystals, is consistent with the d -wave model^{25–27} in the limit of strong (unitary) scattering³¹. Besides, there is nothing foreign in introducing the function $1/\tau(T) \propto T^5$ for the purpose of characterizing scattering in the superconducting state of HTS. A similar temperature dependence of the relaxation rate of quasi-particles follows from the SC model if the phonon corrections to the electromagnetic vertex are taken into account⁹⁵.

In the framework of our modified two-fluid model, the linear low T -dependence of the real part of conductivity $\sigma_1(T)$ is consistent with a constant scattering rate, as it is in a normal metal. While the assumption of a Drude form of the conductivity is supported by the d -wave microscopic analysis³¹, it was shown that pair correlations in the usual impurity scattering models lead to strong T -dependence of the scattering time (neglecting vertex corrections), namely, $\tau(T) \propto T$ in unitary limit, or $\tau(T) \propto 1/T$ in the Born limit. An attempt to resolve this problem in Ref.¹⁶ by choosing an intermediate scattering rate has not provided satisfactory results yet. Very recently the authors of Refs.⁹⁶ and⁹⁷ argue that experimental observation $\sigma_1(T) \propto T$ could be explained by the generalized Drude formula $\sigma_1(T) \propto n_{qp}(T)\tau(T)$ if the quasiparticle density varies as $n_{qp}(T) \propto T$ (as indeed happens for d -wave pairing) and if the effective quasiparticle scattering time $\tau(T)$ saturates at low T . Various possible physical mechanisms of the temperature and energy dependence of τ are discussed in^{96,97}: scattering from the "holes" of the order parameter at impurity sites, and scattering from extended defects. These mechanisms may provide the required saturation of $\tau(T)$ at low T . As was discussed recently in Ref.⁹⁸, the vertex corrections can also modify the low temperature conductivity. However, the temperature dependence has not been investigated yet.

Nevertheless, the microscopic models, which have been investigating the microwave response based on a pure d -wave order parameter symmetry, cannot account for the linear section of the $R_s(T)$ curves extending to $T_c/2$ (at frequencies of 10 GHz and below) in tetragonal HTS single crystals, observation of radically different values of the slopes of $\sigma_2(T)$ for $T \ll T_c$ (corresponding to $\alpha > 1$ in Eq. (20)), observed on YBCO crystals^{8–12}, and unusual features of $\sigma_2(T)$ in the intermediate temperatures range.

Recently, observations of unusual microwave properties of HTS materials have caught the attention of a number of researchers^{43–47,55,56}. These observations are tenta-

tively attributed to mixed ($d + s$)-wave symmetry of the order parameter. Most studies deal with the low temperature variation of the London penetration depth and its relation to an order parameter of mixed symmetry. In particular, it was shown in Ref.⁵⁵ that the low temperature properties of $\lambda(T)$ can be used to distinguish between a pure d -wave order parameter and one with ($s + id$) symmetry, having a small subdominant s -wave contribution in systems connected with a tetragonal lattice. Moreover, additions of impurities suppress the d -wave symmetric part to the benefit of the s -wave part. As a result, a variety of low-temperature dependencies of $\lambda(T)$ is possible for various impurity concentrations, which allows one, in principle, to determine whether or not the order parameter of a superconductor with an orthorhombic lattice is of ($s + id$) or ($s + d$) symmetry⁵³. In Ref.⁴⁶ the ($d + s$) model was generalized to take into account the normal state anisotropy. This is the realistic approach to high- T_c cuprates with an orthorhombic distortion, since recent microwave conductivity data suggest that a substantial part of the ab -anisotropy of $\lambda(T)$ is a normal state effect. It was shown that such an anisotropy affects not only the ab -anisotropy of the transport coefficients, but also the density of states and other thermodynamic quantities. The possible temperature variation of the penetration depth $\lambda(T)$ was analyzed recently in Ref.⁵⁶ in the framework of the ($d + s$) model of hybrid pairing. The slope of the $\Delta\lambda(T) \propto T$ for $T \ll T_c$ and its dependence on the Δ_s/Δ_d admixture in the gap function was analyzed quantitatively, taking into account the impurity scattering. However, the quantitative comparison of the latter calculation with the experimental data has not been performed yet. More interesting discoveries in this field of research can be expected in the near future.

V. ACKNOWLEDGMENTS

We are greatly indebted to N. Bontemps, V. T. Dolgoplov, V. F. Gantmakher, A. A. Golubov, L. M. Fisher, E. G. Maksimov, and V. P. Mineev for many helpful discussions. H. J. F. thanks D. A. Bonn for permission to use the original data points of Ref.¹⁴ in our figures. The research of Yu. A. N. and M. R. T. has been supported by the Russian Fund for Basic Research (grant 97-02-16836) and Scientific Council on Superconductivity (project 96060), and in part by the Program for Russian-Dutch Research Cooperation (NWO).

¹ W. N. Hardy, D. A. Bonn, D. C. Morgan, R. Liang, and K. Zhang, Phys. Rev. Lett. **70**, 3999 (1993).

² D. Achir, M. Poirier, D. A. Bonn, R. Liang, and W. N. Hardy, Phys. Rev. B **48**, 13184 (1993).

- ³ S. Kamal, D. A. Bonn, N. Goldenfeld, P. J. Hirschfeld, R. Liang, and W. N. Hardy, *Phys. Rev. Lett.* **73**, 1845 (1994).
- ⁴ D. A. Bonn, S. Kamal, K. Zhang, R. Liang, D. J. Baar, E. Klein, and W. N. Hardy, *Phys. Rev. B* **50**, 4051 (1994).
- ⁵ J. Mao, D. H. Wu, J. L. Peng, R. L. Greene, and S. M. Anlage, *Phys. Rev. B* **51**, 3316 (1995).
- ⁶ D. A. Bonn, S. Kamal, K. Zhang, R. Liang, and W. N. Hardy, *J. Phys. Chem. Solids* **56**, 1941 (1995).
- ⁷ T. Jacobs, S. Sridhar, C. T. Rieck, K. Scharnberg, T. Wolf, and J. Halbritter, *J. Phys. Chem. Solids* **56**, 1945 (1995).
- ⁸ M. R. Trunin, A. A. Zhukov, G. A. Emel'chenko, and I. G. Naumenko, *Pis'ma Zh. Exp. Teor. Fiz.* **65**, 893 (1997) [*JETP Lett.* **65**, 938 (1997)].
- ⁹ H. Srikanth, B. A. Willemsen, T. Jacobs, S. Sridhar, A. Erb, E. Walker, and R. Flükiger, *Phys. Rev. B* **55**, R14733 (1997).
- ¹⁰ A. A. Zhukov, M. R. Trunin, A. T. Sokolov, and N. N. Kolesnikov, *Zh. Exp. Teor. Fiz.* **112**, 2210 (1997) [*JETP* **85**, 1211 (1997)].
- ¹¹ H. Srikanth, Z. Zhai, S. Sridhar, A. Erb, and E. Walker, *Phys. Rev. B* **57**, 7986 (1998).
- ¹² M. R. Trunin, A. A. Zhukov, and A. T. Sokolov, *J. Phys. Chem. Solids* **59**, 2125 (1998).
- ¹³ S. Kamal, R. Liang, A. Hosseini, D. A. Bonn, and W. N. Hardy, *Phys. Rev. B* **58**, 8933 (1998).
- ¹⁴ A. Hosseini, R. Harris, S. Kamal, P. Dosanjh, J. Preston, R. Liang, W. N. Hardy, and D. A. Bonn, *Phys. Rev. B* **60**, 1349 (1999).
- ¹⁵ L. A. de Vaultier, J. P. Vieren, Y. Guldner, N. Bontemps, R. Combescot, Y. Lemaître, and J. C. Mage, *Europhys. Lett.* **33**, 153 (1996).
- ¹⁶ S. Hensen, G. Müller, C. T. Rieck, and K. Scharnberg, *Phys. Rev. B* **56**, 6237 (1997).
- ¹⁷ S. Djordjević, L. A. de Vaultier, N. Bontemps, J. P. Vieren, Y. Guldner, S. Moffat, J. Preston, X. Castet, M. Guilloux-Viry, and A. Perrin, *Eur. Phys. J. B* **5**, 847 (1998).
- ¹⁸ E. Farber, G. Deutscher, J. P. Contour, and E. Jerby, *Eur. Phys. J. B* **7**, (1999).
- ¹⁹ T. Jacobs, S. Sridhar, Q. Li, G. D. Gu, and N. Koshizuka, *Phys. Rev. Lett.* **75**, 4516 (1995).
- ²⁰ T. Shibauchi, N. Katase, T. Tamegai, and K. Uchinokura, *Physica C* **264**, 227 (1996).
- ²¹ S-F. Lee, D. C. Morgan, R. J. Ormeno, D. M. Broun, R. A. Doyle, and J. R. Waldram, *Phys. Rev. Lett.* **77**, 735 (1996).
- ²² D. V. Shovkun, M. R. Trunin, A. A. Zhukov, N. Bontemps, H. Enriquez, A. Buzdin, and T. Tamegai, to be published.
- ²³ D. M. Broun, D. C. Morgan, R. J. Ormeno, S. F. Lee, A. W. Tyler, A. P. Mackenzie, and J. R. Waldram, *Phys. Rev. B* **56**, R11443 (1997).
- ²⁴ J. R. Waldram, D. M. Broun, D. C. Morgan, R. Ormeno, and A. Porch, *Phys. Rev. B* **59**, 1528 (1999).
- ²⁵ A. Millis, H. Monien, and D. Pines, *Phys. Rev. B* **42**, 167 (1990).
- ²⁶ H. Monien, P. Monthoux, and D. Pines, *Phys. Rev. B* **43**, 275 (1991).
- ²⁷ P. Monthoux, A. Balatsky, and D. Pines, *Phys. Rev. B* **46**, 14803 (1992).
- ²⁸ P. J. Hirschfeld and N. Goldenfeld, *Phys. Rev. B* **48**, 4219 (1993).
- ²⁹ J. P. Carbotte and C. Jiang, *Phys. Rev. B* **48**, 4231 (1993).
- ³⁰ H. Won and K. Maki, *Phys. Rev. B* **49**, 1397 (1994).
- ³¹ P. J. Hirschfeld, W. O. Putikka, and D. J. Scalapino, *Phys. Rev. Lett.* **71**, 3705 (1993); *Phys. Rev. B* **50**, 4051 (1994).
- ³² D. J. Scalapino, *Phys. Rep.* **250**, 329 (1995).
- ³³ J. Annett, N. Goldenfeld, and A. Leggett, in *Physical Properties of High Temperature Superconductors V*, D.M. Ginsberg, eds. (World Scientific, Singapore, 1996).
- ³⁴ K. Maki and H. Won, *J. Phys. I France* **6**, 2317 (1996).
- ³⁵ Yu. A. Izyumov, *Uspekhi Fiz. Nauk*, **167**, 465 (1997); **169**, 225 (1999).
- ³⁶ R. A. Klemm and S. H. Liu, *Phys. Rev. Lett.* **74**, 2343 (1995).
- ³⁷ V. Z. Kresin and S. A. Wolf, *Phys. Rev. B* **41**, 4278 (1990); **46**, 6458 (1992); **51**, 1229 (1995).
- ³⁸ A. A. Golubov, M. R. Trunin, A. A. Zhukov, O. V. Dolgov, and S. V. Shulga, *Pis'ma Zh. Exp. Teor. Fiz.* **62**, 477 (1995) [*JETP Lett.* **62**, 496 (1995)].
- ³⁹ S. D. Adrian, M. E. Reeves, S. A. Wolf, and V. Z. Kresin, *Phys. Rev. B* **51**, 6800 (1995).
- ⁴⁰ M. R. Trunin, *Uspekhi Fiz. Nauk*, **168**, 931 (1998), [*Physics-Uspekhi*, **41**, 843 (1998)].
- ⁴¹ N. Klein, N. Tellmann, H. Schulz, K. Urban, S. A. Wolf, and V. Z. Kresin, *Phys. Rev. Lett.* **71**, 3355 (1993).
- ⁴² Q. P. Li, E. C. Koltenbah, and R. Joynt, *Phys. Rev. B* **48**, 437 (1993).
- ⁴³ R. Combescot and X. Leyronas, *Phys. Rev. Lett.* **75**, 3732 (1995).
- ⁴⁴ C. O' Donovan and J. P. Carbotte, *Phys. Rev. B* **52**, 4568 (1995); **55**, 8520 (1997).
- ⁴⁵ H. Kim and E. J. Nicol, *Phys. Rev. B* **52**, 13576 (1995).
- ⁴⁶ M. T. Beal-Monod and K. Maki, *Phys. Rev. B* **52**, 13576 (1995); **53**, 5775 (1996); **55**, 1194 (1997).
- ⁴⁷ S. V. Pokrovsky and V. L. Pokrovsky, *Phys. Rev. B* **54**, 13275 (1996).
- ⁴⁸ K. A. Musaelian, J. Betouras, A. V. Chubukov, and R. Joynt, *Phys. Rev. B* **53**, 3598 (1996).
- ⁴⁹ Y. Ren, J. Xu, and C. S. Ting, *Phys. Rev. B* **53**, 2249 (1996).
- ⁵⁰ A. A. Shapoval, *Pis'ma Zh. Exp. Teor. Fiz.* **64**, 570 (1996).
- ⁵¹ M. Liu, D. Y. Xing, and Z. D. Wang, *Phys. Rev. B* **55**, 3181 (1997).
- ⁵² E. A. Pashitskii and V. I. Pentegov, *Zh. Exp. Teor. Fiz.* **111**, 298 (1997). [*JETP* **84**, 164 (1997)].
- ⁵³ M. T. Beal-Monod, *Phys. Rev. B* **58**, 8830 (1998); *Physica C* **298**, 59 (1998).
- ⁵⁴ I. Schürer, E. Schachinger, and J.P. Carbotte, *Physica C* **303**, 287 (1998).
- ⁵⁵ R. Modre, I. Schürer, and E. Schachinger, *Phys. Rev. B* **57**, 5496 (1998).
- ⁵⁶ Yu. A. Nefyodov, A. A. Golubov, M. R. Trunin, and M. T. Beal-Monod, to be published in *Physica B*.
- ⁵⁷ D. A. Bonn, P. Dosanjh, R. Liang, and W. N. Hardy, *Phys. Rev. Lett.* **68**, 2390 (1992).
- ⁵⁸ K. Zhang, D. A. Bonn, R. Liang, D. J. Baar, and W. N. Hardy, *Appl. Phys. Lett.* **62**, 3019 (1993).
- ⁵⁹ D. A. Bonn, R. Liang, T. M. Riseman, D. J. Baar, D. C. Morgan, K. Zhang, P. Dosanjh, T. L. Duty, A. Mac-

- Farlane, G. D. Morris, J. H. Brewer, W. N. Hardy, C. Kallin, and A. J. Berlinsky, Phys. Rev. B **47**, 11314 (1993).
- ⁶⁰ H. Kitano, T. Shibauchi, K. Uchinokura, A. Maeda, H. Asaoka, and H. Takei, Phys. Rev. B **51**, 1401 (1995).
- ⁶¹ M. R. Trunin, J. Superconductivity **11**, 381 (1998).
- ⁶² S. M. Quinlan, D. J. Scalapino, and N. Bulut, Phys. Rev. B **49**, 1470 (1994).
- ⁶³ G. M. Eliashberg, *Zh. Exp. Teor. Fiz.* **38**, 966 (1960) [JETP **11**, 696 (1960)]; *Pis'ma Zh. Exp. Teor. Fiz.* **48**, 275 (1988).
- ⁶⁴ W. E. Pickett, J. Superconductivity **4**, 397 (1991).
- ⁶⁵ V. L. Ginzburg and E. G. Maksimov, *Sverkhprovodimost': Fiz., Khim., Tekh.* **5**, 1543 (1992).
- ⁶⁶ A. A. Golubov, M. R. Trunin, A. A. Zhukov, O. V. Dolgov, and S. V. Shulga, J. Phys. I France **6**, 2275 (1996).
- ⁶⁷ A. Bille and K. Scharnberg, J. Phys. Chem. Solids **59**, 2110 (1998).
- ⁶⁸ C. M. Varma, P. B. Littlewood, S. Schmitt-Rink, E. Abrahams, and A. E. Ruskenshtein, Phys. Rev. Lett. **63**, 1996 (1989).
- ⁶⁹ E. Abrahams, J. Phys. I France **6**, 2191 (1996).
- ⁷⁰ P. W. Anderson, *Physica C* **185-189**, 11 (1991).
- ⁷¹ P. W. Anderson, *Theory of Superconductivity in the High- T_c Cuprates* (Princeton: Princeton University Press, 1997).
- ⁷² P. A. Lee, Phys. Rev. Lett. **71**, 1887 (1993).
- ⁷³ M. R. Trunin, A. A. Zhukov, G. E. Tsydynzhapov, A. T. Sokolov, L. A. Klinkova, and N. V. Barkovskii, *Pis'ma Zh. Exp. Teor. Fiz.* **64**, 783 (1996) [JETP Lett. **64**, 832 (1996)].
- ⁷⁴ H. J. Fink, Phys. Rev. B **58**, 9415 (1998); H. J. Fink, unpublished.
- ⁷⁵ H. J. Fink and M. R. Trunin, to be published in Physica B.
- ⁷⁶ C. S. Gorter and H. Casimir, *Phys. Z.* **35**, 963 (1934).
- ⁷⁷ M. R. Trunin, to be published in Physica B.
- ⁷⁸ N. E. Glass and W. F. Hall, Phys. Rev. B **44**, 4495 (1991).
- ⁷⁹ H. K. Olsson and R. H. Koch, Phys. Rev. Lett. **68**, 2406 (1992).
- ⁸⁰ A. A. Golubov, M. R. Trunin, S. V. Shulga, D. Wehler, J. Dreiholz, G. Müller, and H. Piel, Physica C **213**, 139 (1993).
- ⁸¹ M. L. Horbach, W. van Saarloos, and D. A. Huse, Phys. Rev. Lett. **67**, 3464 (1991).
- ⁸² S. M. Anlage, J. Mao, J. C. Booth, D. H. Wu, and J. L. Peng, Phys. Rev. B **53**, 2792 (1996).
- ⁸³ G. M. Eliashberg, *Zh. Exp. Teor. Fiz.* **39**, 1437 (1960) [JETP **12**, 1000 (1961)].
- ⁸⁴ A. E. Karakozov, E. G. Maksimov, and S. A. Mashkov, *Zh. Exp. Teor. Fiz.* **68**, 1937 (1975) [JETP **41**, 971 (1976)].
- ⁸⁵ F. Marsiglio, Phys. Rev. B **44**, 5373 (1991).
- ⁸⁶ A. E. Karakozov, E. G. Maksimov, and A. A. Mikhailovskii, *Zh. Exp. Teor. Fiz.* **102**, 132 (1992) [JETP **75** (1), 70 (1992)].
- ⁸⁷ O. V. Dolgov, E. G. Maksimov, A. E. Karakozov, and A. A. Mikhailovsky, Solid State Comm. **89**, 827 (1994).
- ⁸⁸ G. V. Klimovich, A. V. Rylyakov, and G. M. Eliashberg, *Pis'ma Zh. Exp. Teor. Fiz.* **53**, 381 (1991) [JETP Lett. **53**, 399 (1991)].
- ⁸⁹ A. A. Mikhailovsky, S. V. Shulga, A. E. Karakozov, O. V. Dolgov, and E. G. Maksimov, Solid State Comm. **80**, 511 (1991).
- ⁹⁰ R. T. Collins, Z. Schlesinger, F. Holtzberg, C. Field, U. Welp, G. W. Crabtree, J. Z. Liu, and Y. Fang, Phys. Rev. B **43**, 3701 (1991).
- ⁹¹ J. Rammer, Europhys. Lett. **5**, 77 (1991).
- ⁹² A. Andreone, C. Cantoni, A. Cassinese, A. Di Chiara, and R. Vaglio, Phys. Rev. B **56**, 7874 (1997).
- ⁹³ E. G. Maksimov, D. Yu. Savrasov, and S. Yu. Savrasov, *Uspekhi Fiz. Nauk*, **167**, 354 (1997).
- ⁹⁴ M. R. Trunin, A. A. Zhukov, and A. T. Sokolov, *Zh. Exp. Teor. Fiz.* **111**, 696 (1997) [JETP **84**, 383 (1997)].
- ⁹⁵ G. M. Eliashberg, G. V. Klimovich, and A. V. Rylyakov, J. Supercond. **4**, 393 (1991).
- ⁹⁶ M. H. Hettler and P. J. Hirschfeld, preprint cond-mat/9907150, unpublished.
- ⁹⁷ A. J. Berlinsky, D. A. Bonn, R. Harris, and C. Kallin, preprint cond-mat/9908159, unpublished.
- ⁹⁸ A. C. Durst and P. A. Lee, preprint cond-mat/9908182, unpublished.